the measured T_0's is allowed. For additional information, the reader is referred to Ref. 5.

[1] N. Rynn, Phys. Fluids 5, 635 (1962).
[2] S. von Göler, Phys. Fluids 7, 463 (1964).
[3] E. Hinnov, J. G. Hirschberg, F. W. Hofmann, and N. Rynn, Princeton University, Plasma Physics Laboratory Report Matt-206 (1963).
[4] A. Y. Wong and A. F. Kuckes, Phys. Rev. Letters 13, 306 (1964).
[5] N. D'Angelo and A. Y. Wong, Princeton University, Plasma Physics Laboratory Report, Matt-284 (1964).

Approximate Method for the Determining of Bubble Dynamics in Non-Newtonian Fluids

WEN-JEI YANG
AND
HSU-CHIEH YEH
The University of Michigan, Ann Arbor, Michigan
(Received 27 March 1964; final manuscript received 27 November 1964)

AN approximate method is developed to determine the time-history of the bubble size, pressure distribution and energy-dissipation rate in an incompressible, non-Newtonian fluid having an arbitrary stress–strain relationship.

Consider a spherical bubble growing or collapsing in an infinite mass of homogeneous incompressible liquid. In an absence of body forces, the equations of continuity and motion in the liquid may be expressed in spherical coordinates as

$$\frac{1}{r^2}\frac{\partial}{\partial r}(r^2u) = 0 \tag{1}$$

and

$$\rho_l\left(\frac{\partial u}{\partial t} + u\frac{\partial u}{\partial r}\right) = -\frac{\partial p}{\partial r} - \left[\frac{1}{r^2}\frac{\partial}{\partial r}(r^2\tau_{rr}) - \frac{\tau_{\theta\theta} - \tau_{\phi\phi}}{r}\right], \tag{2}$$

respectively,[1] where r is the distance from the center of the bubble; u, the radial velocity at r; ρ_l, the density of liquid; p, the pressure; and τ_{rr}, $\tau_{\theta\theta}$, and $\tau_{\phi\phi}$ the viscous normal stresses in the directions of r, θ, and ϕ respectively.

If the vapor density inside the bubble is assumed very small compared with ρ_l, and R and $\dot{R}$ represent the instantaneous bubble radius and its expansion rate then the integration of equation (1) yields

$$u = R^2\dot{R}/r^2. \tag{3}$$

For a Newtonian fluid with the normal stresses given as $\tau_{rr} = -2\tau_{\theta\theta} = -2\tau_{\phi\phi} = 4\mu R^2\dot{R}/r^3$, the substitution of Eq. (3) into Eq. (2) followed by an integration from $r = r$ to $r = \infty$ yields

$$\rho_l\left[\frac{\ddot{R}R^2}{r} + \frac{\dot{R}^2R}{r}\left(2 - \frac{R^3}{2r^3}\right)\right] = p_l(r) - p_l(\infty). \tag{4}$$

Similarly for the Bingham-plastic model with $\tau_{rr} = -2\tau_{\theta\theta} = -2\tau_{\phi\phi} = 4\eta(R^2\dot{R}/r^3) \pm (2/\sqrt{3})\tau_0$ as its normal stresses, the integration form $r = r$ to $r = r_0$ gives

$$\rho_l\left[\ddot{R}R^2\left(\frac{1}{r} - \frac{1}{r_0}\right) + \dot{R}^2\left(\frac{R^4}{2r_0^4} - \frac{R^4}{2r^4} + \frac{2R}{r} - \frac{2R}{r_0}\right)\right] = p_l(r) - p_l(r_0) \mp 2\sqrt{3}\tau_0 \ln\frac{r_0}{r}, \tag{5}$$

where the upper sign is for $\dot{R} \geq 0$ and lower sign is for $\dot{R} \leq 0$. However, in many actual non-Newtonian fluids, the expression for the stress–strain relationship is either not available or too complicated. It is the purpose of this note to demonstrate that the solution of this problem may be obtained by the piecewise fit of linear approximations to the shear-stress–shear-strain diagram of any arbitrary form. Let the actual curve be approximated by $n + 1$ linear combinations, 0, 1, 2, 3, ... , n as shown in Fig. 1 (a). The slope of each is μ, η_1, η_2, ... , η_n. Then the first line $j = 0$ represents the rheological behavior of a Newtonian fluid with viscosity μ and the $(i + 1)$th section $j = i$ represents that of a Bingham plastic with the yield stress τ_i and the coefficient of rigidity η_i. Since the expressions for the shear and normal stresses are respectively $\tau_{yx} = -\mu(du/dy)$ and $\tau_{rr} = -2\mu(du/dr)$ for a Newtonian fluid; $\tau_{yx} = -\eta(du/dy) \pm \tau_0$ and $\tau_{rr} = -2\eta(du/dy) \pm (2/\sqrt{3})\tau_0$ for a Bingham plastic; a plot of τ_{rr} vs $(-du/dr)$ which is analogous to Fig. 1 (a) for τ_{yx} vs $(-du/dy)$ is constructed as shown in Fig. 1 (b). This step of converting the shear-stress–shear-strain diagram to the normal-stress–shear-strain diagram is necessary because the experimental results are available for the former diagram, while the present analysis utilizes the latter. The differentiation of Eq. (3) gives

$$-du/dr = 2R^2\dot{R}/r^3$$

an expression for the rate of shear at r. It signifies that at any instant there is a location r_i in the fluid where its rate of shear is equal to $C_i/\sqrt{3}$. The location is

$$r_i = (2\sqrt{3}R^2\,|\dot{R}|/C_i)^{\frac{1}{3}} \quad \text{for} \quad i = 0, 1, 2, \ldots, n.$$

Based on this relationship, the fluid may be considered to consist of $n + 2$ regions between R and infinity, that is, $R \leq r \leq r_n$, $r_n \leq r \leq r_{n-1}$, ... , $r_0 \leq r \leq \infty$. The rheological behavior of the fluid in each region is represented by a line approximating

the actual curve in Fig. 1 (a). For example, the fluid in the region $r_0 \leq r \leq \infty$ behaves as a Newtonian fluid with the viscosity μ, while that in the region $r_{i+1} \leq r \leq r_i$ behaves as a Bingham plastic with the yield stress τ_i and the coefficient of rigidity η_i. The substitutions of $r = r_{i+1}$, $r_0 = r_i$ for $i = 0, 1, 2, \ldots, m-2$ and $r = r$, $r_0 = r_{m-1}$ into Eq. (5) yield

$$\rho_l\left\{\ddot{R}R^2\left(\frac{1}{r_{i+1}} - \frac{1}{r_i}\right) + \dot{R}^2\left[2R\left(\frac{1}{r_{i+1}} - \frac{1}{r_i}\right) - \frac{R^4}{2}\left(\frac{1}{r_{i+1}^4} - \frac{1}{r_i^4}\right)\right]\right\} = p_l(r_{i+1}) - p_l(r_i) \mp 2\sqrt{3}\tau_i \ln (r_i/r_{i+1}), \quad \text{for } i = 0, 1, 2, \ldots, m-2,$$

$$\rho_l\left\{\ddot{R}R^2\left(\frac{1}{r} - \frac{1}{r_{m-1}}\right) + \dot{R}^2\left[2R\left(\frac{1}{r} - \frac{1}{r_{m-1}}\right) - \frac{R^4}{2}\left(\frac{1}{r^4} - \frac{1}{r_{m-1}^4}\right)\right]\right\} = p_l(r) - p_l(r_{m-1}) \mp 2\sqrt{3}\tau_{m-1} \ln (r_{m-1}/r), \quad \text{for } R \leq r \leq r_{m-1}, \tag{6}$$

respectively. Equations (6) provide m equations for the m regions $r_1 \leq r \leq r_0$, $r_2 \leq r \leq r_1$, $\ldots$, $R \leq r \leq r_{m-1}$. In the last region $r_0 \leq r \leq \infty$, Eq. (4) with r replaced by r_0 represents the equation of motion. Now the m equations as described by Eqs. (6) are combined with Eq. (4) to eliminate the m unknown quantities $p_l(r_i)$. This yields

$$\rho_l\left[\frac{\ddot{R}R^2}{r} + R^2\left(\frac{2R}{r} - \frac{R^4}{2r^4}\right)\right] = p_l(r) - p_l(\infty) \mp 2\sqrt{3}\left(\tau_{m-1} \ln \frac{r_{m-1}}{r} + \sum_{i=0}^{m-2} \tau_i \ln \frac{r_i}{r_{i+1}}\right), \tag{7}$$

which is the equation for the pressure distribution in the immediate vicinity of the growing or collapsing bubble. The balance of force at the bubble wall requires that

$$p_l(R) + 2\sigma/R + \tau_{rr,l}(R) = p_g(R) - \tau_{rr,g}(R), \tag{8}$$

where $p_g(R)$ is the gas pressure inside the bubble at the immediate vicinity of the bubble surface, σ is the surface tension, and $\tau_{rr,l}$ and $\tau_{rr,g}$ are the radial normal stresses acting on the bubble surface due to the liquid and gaseous-phase viscosities, respectively. If the gas inside the bubble is assumed a Newtonian fluid, then

$$\tau_{rr,g}(R) = -2\mu_g(\partial u/\partial r)_{r=R} = 4\mu_g\dot{R}/R. \tag{9}$$

The dynamic equation for the growth or collapse of the bubble may then be obtained from equation (7) by replacing r by R or in terms of $p_g(R)$ as

$$\rho_l(\ddot{R}R + 3\dot{R}^2/2) = p_g(R) - p_l(\infty) - 2\sigma/R - 4(\eta_{m-1} + \mu_g)\dot{R}/R \mp 2\sqrt{3}\left(\tfrac{1}{3}\tau_{m-1} + \sum_{i=0}^{m-2} \tau_i \ln \frac{r_i}{r_{i-1}}\right). \tag{10}$$

The appropriate initial conditions are $R(0) = R_0$ and $\dot{R}(0) = 0$ where R_0 is the initial size of the bubble. The rate of energy dissipation in the liquid, defined as $-(\boldsymbol{\tau} : \nabla\mathbf{v})$ per unit volume, is

$$-\sum_{i=0}^{m-1}\int_{r_{i+1}}^{r_i} (\boldsymbol{\tau}_i : \nabla\mathbf{v})4\pi r^2\, dr - \int_{r_0}^{\infty} (\boldsymbol{\tau}_N : \nabla\mathbf{v})4\pi r^2\, dr = 16\pi R^4\dot{R}^2\left[\frac{\mu_l}{r_0^3} + \sum_{i=0}^{m-1}\eta_i\left(\frac{1}{r_{i+1}^3} - \frac{1}{r_i^3}\right)\right] \pm 8\sqrt{3}\pi R^2\dot{R}\sum_{i=0}^{m-1}\tau_i \ln \frac{r_i}{r_{i+1}}, \tag{11}$$

where r_m corresponds to the bubble radius R, $\boldsymbol{\tau}_i$ and $\boldsymbol{\tau}_N$ are the stress tensors for a Bingham-plastic in the region $r_i \geq r \geq r_{i+1}$ and a Newtonian fluid in the region $r_0 \leq r \leq \infty$, respectively, and $\mathbf{v}$ is a velocity vector.

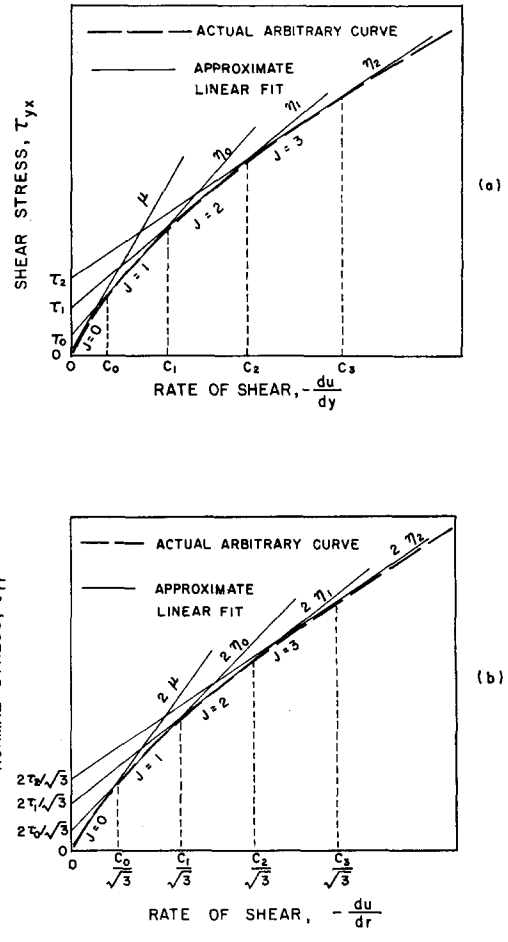

FIG. 1. Stress–strain diagrams.

The time-history of bubble size and its velocity resulting from a disturbance $p_g(R) - p_l(\infty)$ may be obtained by the numerical reduction of Eq. (10) with the appropriate initial conditions by means of the Runge–Kutta method. Then R, $\dot{R}$, and $\ddot{R}$ are substituted into Eqs. (7) and (11) for the numerical evaluation of the pressure distribution near the bubble and the energy-dissipation rate in the liquid.

The work was supported by the Du Pont Grant for Basic Research in Mechanical Engineering.

[1] R. B. Bird, W. E. Stewart, and E. N. Lightfoot, *Transport Phenomena* (John Wiley & Sons, Inc., New York, 1960), Chap. 3.

Reduction of Velocity Fluctuations in a Kármán Vortex Street by a Vibrating Cylinder

O. H. Wehrmann
Boeing Scientific Research Laboratories, Seattle, Washington
(Received 3 August 1964; final manuscript received 7 December 1964)

THE effect of a compliant wall on the transition from laminar to turbulent flow has been treated by Krämer,[1] Benjamin,[2] Landahl,[3] and Hains.[4] Another case of instability which leads to the well-known Kármán vortex street occurs in the laminar wake behind a cylinder. This note describes the results of an experiment to determine the effect of induced vibration of the cylinder on the intensity of the velocity fluctuations in the street.

Roshko[5] has shown that the flow phenomena behind the cylinder can be described by three different regimes of the Reynolds number based on the cylinder diameter. For Re $<$ 40 the wake is steady and laminar; while for 40 $<$ Re $<$ 160 the wake is unstable for small disturbances, and a vortex street with a distinct frequency develops. As the Reynolds number is increased beyond 160, the wake becomes turbulent. Thus, for the range 40 $<$ Re $<$ 160, the influence of induced vibrations of the cylinder in the laminar wake is of interest. At the present time there exists no satisfactory theory for the development of the Kármán vortex street. The shedding frequency f is only given by an empirical law by Roshko[5]

$$fd^2/\nu = 0.212(Ud/\nu) - 4.5, \qquad (1)$$

where d is the diameter of the circular cylinder, U the flow velocity, and ν the kinematic viscosity. This law was found to apply also in the case of an obround cylinder used in the experiment, if d is taken to be the width.

In an experiment it is desired to satisfy the following conditions: (1) The vibrations of the cylinder should be induced by external means, and the frequency should be adjustable without changing the Reynolds number or size of the cylinder. (2) The amplitude and the phase of the vibrations should be adjustable with reference to the amplitude and phase of the velocity fluctuations in the vortex street. The first requirement is satisfied by making the cylinder out of a piezoelectric material whose shape depends on the applied voltage. The second requirement is satisfied by the use of a special electronic feedback system because measurements with an independent source in the form of an ac generator have shown that, in this case, no reduction could be obtained because of the uncorrelated phase relation between vibrations and velocity fluctuations.

The experimental arrangement is shown in Fig. 1. The Clevite PZT Bimorph cylinder has an obround shape—0.154 cm long and 0.0675 cm wide. By applying an ac voltage to the cylinder, vibrations with well-controlled amplitude in the frequency range from 20 cps to 500 kcps were obtained. It should be mentioned that the cylinder vibrated by changing its cross-sectional shape, so that the axis of the cylinder was fixed.

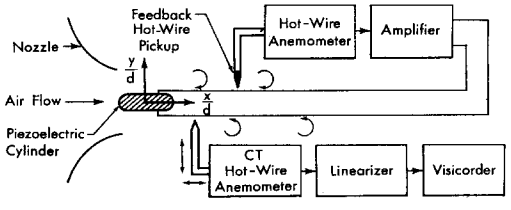

FIG. 1. The experimental arrangement.

The cylinder was placed in a low-turbulence laminar jet with its longer side in the flow direction, to produce a vortex street. Two constant temperature hot-wire sets were used. The output of the first hot-wire set was fed to an amplifier to drive the cylinder with the shedding frequency of the vortices. In this way, a feedback system was formed. The phase of the cylinder vibrations with reference to the traveling vortices was varied by changing the position of the hot-wire along the vortex street, and the amplitude was controlled by the degree of amplification. The second hot-wire, whose position could be varied, was used to measure the amplitude of the fluctuations produced by the vortices. The linearized signal was fed into a recorder for evaluation. It was observed that the frequency was not influenced, but a significant reduction in the amplitude of the fluctuations could be obtained with the proper selection of the phase and amplitude of the feedback system.

The following results have been obtained for